



FULL LENGTH ARTICLE

The endoplasmic reticulum membrane protein complex subunit *Emc6* is essential for rhodopsin localization and photoreceptor cell survival



Kuanxiang Sun ^{a,b,c,d}, Lu Liu ^c, Xiaoyan Jiang ^c, Heting Wang ^a,
Lin Wang ^c, Yeming Yang ^c, Wenjing Liu ^c, Lin Zhang ^c,
Xiaohui Zhao ^{b,*}, Xianjun Zhu ^{a,b,c,d,e,*}

^a Health Management Center, Sichuan Provincial People's Hospital, University of Electronic Science and Technology of China, Chengdu, Sichuan 610072, China

^b Key Laboratory of Tibetan Medicine Research, Chinese Academy of Sciences and Qinghai Provincial Key Laboratory of Tibetan Medicine Research, Northwest Institute of Plateau Biology, Xining, Qinghai 810008, China

^c The Sichuan Provincial Key Laboratory for Human Disease Gene Study and Department of Laboratory Medicine, Center for Medical Genetics, Sichuan Provincial People's Hospital, University of Electronic Science and Technology of China, Chengdu, Sichuan 610072, China

^d Research Unit for Blindness Prevention of Chinese Academy of Medical Sciences (2019RU026), Sichuan Academy of Medical Sciences and Sichuan Provincial People's Hospital, Chengdu, Sichuan 610072, China

^e Department of Ophthalmology, The First People's Hospital of Shangqiu, Shangqiu, Henan 476000, China

Received 21 September 2022; received in revised form 17 February 2023; accepted 29 March 2023
Available online 23 May 2023

KEYWORDS

ANO2;
Cilium;
EMC6;
ER membrane protein complex;
Mislocalization;
Photoreceptor

Abstract The endoplasmic reticulum (ER) membrane protein complex (EMC) is responsible for monitoring the biogenesis and synthetic quality of membrane proteins with tail-anchored or multiple transmembrane domains. The EMC subunit EMC6 is one of the core members of EMC and forms an enclosed hydrophilic vestibule in cooperation with EMC3. Despite studies demonstrating that deletion of EMC3 led to rhodopsin mislocalization in rod photoreceptors of mice, the precise mechanism leading to the failure of rhodopsin trafficking remains unclear. Here, we generated the first rod photoreceptor-specific knockout of *Emc6* (RKO) and cone photoreceptor-specific knockout of *Emc6* (CKO) mouse models. Deficiency of *Emc6* in rod

* Corresponding author.

E-mail addresses: xhzhao@nwpb.cas.cn (X. Zhao), xjzhu@uestc.edu.cn (X. Zhu).

Peer review under responsibility of Chongqing Medical University.

<https://doi.org/10.1016/j.gendis.2023.03.033>

2352-3042/© 2023 The Authors. Publishing services by Elsevier B.V. on behalf of KeAi Communications Co., Ltd. This is an open access article under the CC BY-NC-ND license (<http://creativecommons.org/licenses/by-nc-nd/4.0/>).

degeneration;
TMEM67

photoreceptors led to progressive shortening of outer segments (OS), impaired visual function, mislocalization and reduced expression of rhodopsin, and increased gliosis in rod photoreceptors. In addition, CKO mice displayed the progressive death of cone photoreceptors and abnormal localization of cone opsin protein. Subsequently, proteomics analysis of the RKO mouse retina illustrated that several cilium-related proteins, particularly anoctamin-2 (ANO2) and transmembrane protein 67 (TMEM67), were significantly down-regulated prior to OS degeneration. Detrimental rod photoreceptor cilia and mislocalized membrane disc proteins were evident in RKO mice. Our data revealed that in addition to monitoring the synthesis of rhodopsin-dominated membrane disc proteins, EMC6 also impacted rod photoreceptors' ciliogenesis by regulating the synthesis of membrane proteins associated with cilia, contributing to the mislocalization of membrane disc proteins.

© 2023 The Authors. Publishing services by Elsevier B.V. on behalf of KeAi Communications Co., Ltd. This is an open access article under the CC BY-NC-ND license (<http://creativecommons.org/licenses/by-nc-nd/4.0/>).

Introduction

Gradual degeneration of photoreceptors is the major characteristic of retinitis pigmentosa, which is a heterogeneous disorder, leading to severe visual impairment and eventually to blindness.^{1–4} Mutants of rhodopsin, a protein essential to rod photoreceptors, account for approximately 25% of autosomal dominant retinitis pigmentosa cases.⁵ A large majority of these mutations disrupt rhodopsin trafficking from the endoplasmic reticulum (ER) to the plasma membrane.⁶ Defects in biosynthesis and trafficking of rhodopsin cause failure to function and death of rod photoreceptors.^{7,8}

The outer segment (OS) of photoreceptors is mainly involved in phototransduction, yet all protein syntheses in the photoreceptors occur in the inner segment (IS). Thus, protein transport from IS to OS is particularly important for the survival and function of photoreceptor cells.^{9,10} The OS of rod and cone photoreceptors was generally regarded as a highly modified and specialized primary cilium. The IS and OS of photoreceptors were connected by connecting cilia (CC), which are homologous to the transition zone (TZ) of the primary cilium. As a structure composed of microtubules, the CC consists of an axoneme with nine doublet microtubules nucleated by a triplet microtubule basal body (BB). The CC acts as a conduit for transporting photopigment molecules, phototransduction proteins, and disc phospholipids from the IS to the OS in photoreceptors.¹¹ In the presence of ciliary dysfunction, specific proteins necessary for the development and maintenance of the photoreceptor OS are disrupted, resulting in photoreceptors' degeneration.

The ER membrane protein complex (EMC), as a conserved complex in membrane protein biogenesis, was originally discovered in yeast, with six subunits (EMC1–EMC6).¹² Ten subunits of EMC (EMC1–EMC10) were subsequently identified in mammals. EMC was initially demonstrated to be a transmembrane domain insertion enzyme for tail-anchored membrane proteins and multi-pass membrane proteins by functional investigations of knockout strains *in vivo* and recombinant liposomes *in vitro*.^{13,14} The largest subunit EMC1 plays roles in the transport of polyomavirus SV40, the entry of ER Ca²⁺, and

the development of congenital neural crest in *Xenopus*.^{15–17} Variants in *EMC1* were associated with retinal diseases.^{18,19} More recently, other mutations in *EMC1* were reported to be associated with autism disorder, global developmental delay, and visual impairment.^{20,21} *Emc3* is essential for the biogenesis and homeostasis of rhodopsin, a multi-pass G protein-coupled receptor (GPCR) membrane protein in rod photoreceptor cells.^{22,23} However, whether other subunits of the EMC play similar roles remains unknown.

EMC6, also named transmembrane protein 93, is an indispensable subunit of EMC.²⁴ Initially, EMC6 was discovered to be involved in the synthesis of ionotropic acetylcholine and γ -Aminobutyric acid type A (GABA_A) receptors in *Caenorhabditis elegans*.²⁵ Subsequently, EMC6 was discovered to be a novel positive cellular autophagy regulator.²⁶ Recently, EMC6 was revealed to induce apoptosis and inflammatory damage in glandular follicle cells by proteomic analysis in the progression of pancreatitis.²⁷ Nevertheless, the function of EMC6 in the retinal photoreceptor cells is still poorly understood.

In this study, we generated rod and cone-specific *Emc6* knockout models to assess the roles of *Emc6* in the retinal photoreceptor cells. Deletion of *Emc6* in rod cells resulted in early-onset retinal degeneration and mislocalization of rhodopsin and other membrane disc proteins. Our data highlight the essential role of EMC6 in the synthesis and transport of rhodopsin in retinal photoreceptors.

Materials and methods

Mice and genotyping

All experimental protocols for animal studies were approved by the Animal Care and Use Committee of Sichuan Provincial People's Hospital and were performed according to the ARVO Statement for the Use of Animals in Ophthalmic and Vision Research. All animals were housed in a specific pathogen-free barrier facility with a 12-h light/12-h dark cycle.

Emc6 floxed mice (*Emc6*^{flox/flox}, named *Emc6*^{em1xzhu}) were engineered on the C57BL/6J genetic background using

the CRISPR/Cas9 system. The first loxP site was inserted in intron 2, while the second loxP site was inserted in intron 3, 673bp downstream of the first loxP site. To generate rod cell-specific and cone cell-specific *Emc6* knockout mice, homozygous (*Emc6*^{flox/flox}) mice were mated to Rhodopsin-iCre (Rod-Cre) and Cone-Cre mice to yield heterozygous progeny.²⁸ The heterozygous progenies were mated to *Emc6*^{flox/flox} mice to obtain *Emc6*^{flox/flox}; Rod-Cre mice (designated RKO mice) (Fig. S1A) and *Emc6*^{flox/flox}; Cone-Cre mice (designated CKO mice) (Fig. S1B). *Emc6*^{flox/flox} mice, designated as wild-type (WT) mice, were used as the control group in the follow-up experiment.

Genomic DNA templates obtained from mouse tails were used to genotype mice by polymerase chain reaction (PCR) with the corresponding primers (Table S1). The PCR protocol for *Emc6* floxed mice consisted of 95 °C for 5 min, followed by 35 cycles of 95 °C for 30 s, 60 °C for 30 s, and 72 °C for 30 s, and 1 cycle of 72 °C for 5 min. For Rod-Cre mice, the first cycle consisted of 94 °C for 3 min, followed by 35 cycles of 95 °C for 30 s, 60 °C for 30 s, and 72 °C for 45 s, and 1 cycle of 72 °C for 5 min. For Cone-Cre mice, the first cycle consisted of 95 °C for 5 min, followed by 35 cycles of 95 °C for 15 s, 60 °C for 15 s, and 72 °C for 20 s, and 1 cycle of 72 °C for 5 min.

Reverse transcription quantitative real-time PCR (RT-qPCR)

Total RNA was extracted as described previously. Total RNA was reverse transcribed into cDNA using a reverse transcription kit (Ambion, Austin, TX, USA, 18090010). Quantitative real-time PCR was performed using an SYBR Green kit (Bio-Rad Laboratories, USA, KK4607), and transcript levels were normalized to GAPDH. The corresponding primers used for RT-qPCR were listed in Table S1.

Histological staining and measurement of the outer nuclear layer (ONL)

For hematoxylin and eosin staining (H&E), enucleated eyes from 30-, 50-, and 120-day-old mice were rinsed in PBS, fixed overnight in buffer containing 1.22% glutaraldehyde and 0.8% paraformaldehyde. Eyes were embedded in paraffin in the same direction to ensure the same eccentricity of the sections. Eyes were cut into 8- μ m-thick sections. Sections showing the central location of the optic nerve were then taken for H&E staining. The thickness of ONL was measured every 400 μ m from the optic nerve. The thickness of ONL from 3 WT to 3 RKO mice was counted separately.

Electroretinogram (ERG) recording

50-day-old WT and RKO mice were dark-adapted for 6 h, and all follow-up experiments were conducted in a dark environment. Mice were anesthetized with saline containing ketamine and xylazine. Pupils were then dilated with 1% tropicamide. The scotopic ERG responses were recorded and analyzed simultaneously from both eyes using an instrument set of Roland electroretinogram recorder and Ganzfeld Q450 stimulator (Roland Consult, Heidelberg, Germany). Dark-adapted ERGs were recorded with intensities ranging from 0.01 to 10 cd·s/m².

Transmission electron microscopy (TEM)

Fresh retinal tissues were prefixed with a 3% glutaraldehyde and 1% osmium tetroxide. The retinal tissues were dehydrated in a series of acetone. Then they were infiltrated in Epon 812 for 1 h and then embedded in fresh Epon 812 solution for 10 h. Semithin sections were optically positioned with methylene blue staining and cut with a diamond knife to yield 60–70 nm ultrathin sections, which were stained with uranyl acetate for 45 min and lead citrate for 5 min. TEM images were acquired on a JEM-1400-Flash machine.

Western blotting

Mouse retinal tissues were harvested and lysed in standard RIPA lysis buffer (Beyotime Biotechnology, Beijing, China) containing ethylenediaminetetraacetic acid (EDTA)-free protease inhibitor cocktail (TransGen, Beijing, China), sonicated five times for 3 s and centrifuged at 10,000 g for 10 min at low temperature. Equal amounts of protein were loaded onto SDS-polyacrylamide gel (10% or 12.5%), then separated by electrophoresis and transferred to nitrocellulose (NC) membranes. Skim milk powder dissolved in a buffer containing 0.1% Tween 20 (TBST) to produce an 8% blocking solution. The NC membranes were blocked with an 8% blocking solution for 1–2 h and then incubated with primary antibodies overnight. The primary antibodies used were shown in Table S2. The NC membranes were washed with TBST and incubated with secondary antibodies for 1–2 h. Protein signals were detected using a SuperSignal West Pico Chemiluminescent Substrate (Thermo Fisher Scientific). The relative density of the protein was calculated by ImageJ software.

Immunohistochemistry

For immunohistochemistry, eyes from 30-, 50-, and 120-day-old mice were enucleated and an incision was made in the center of the cornea. Eyes were fixed in 4% paraformaldehyde (PFA) in 100 mM phosphate buffer (PBS) for 2 h and dehydrated in 30% sucrose for 2 h. After the lens were removed, the eyes were immersed in OCT and immediately frozen at –80 °C for sectioning. The frozen eyes were cut into 10- μ m-thick sections, then blocked and permeabilized with 10% normal bovine serum and 0.2% Triton X-100 for 2 h. The slides were incubated overnight with various primary antibodies which were shown in Table S2. Subsequently, the sections were stained with secondary antibodies (Life Technologies, USA), Peanut Agglutinin (PNA) (RL-1072-5, Vector Laboratories, USA), and DAPI for 2 h. TUNEL staining was performed using the In Situ Cell Death Detection Kit (Roche, Redwood City, CA, USA) according to the standard protocol. Fluorescence images were captured by LSM 800 confocal laser scanning microscope (LSM800, Carl Zeiss, Germany).

Proteomic analysis

Proteomic analysis was performed on three independent biological replicates from WT and RKO retinas at 4 weeks of

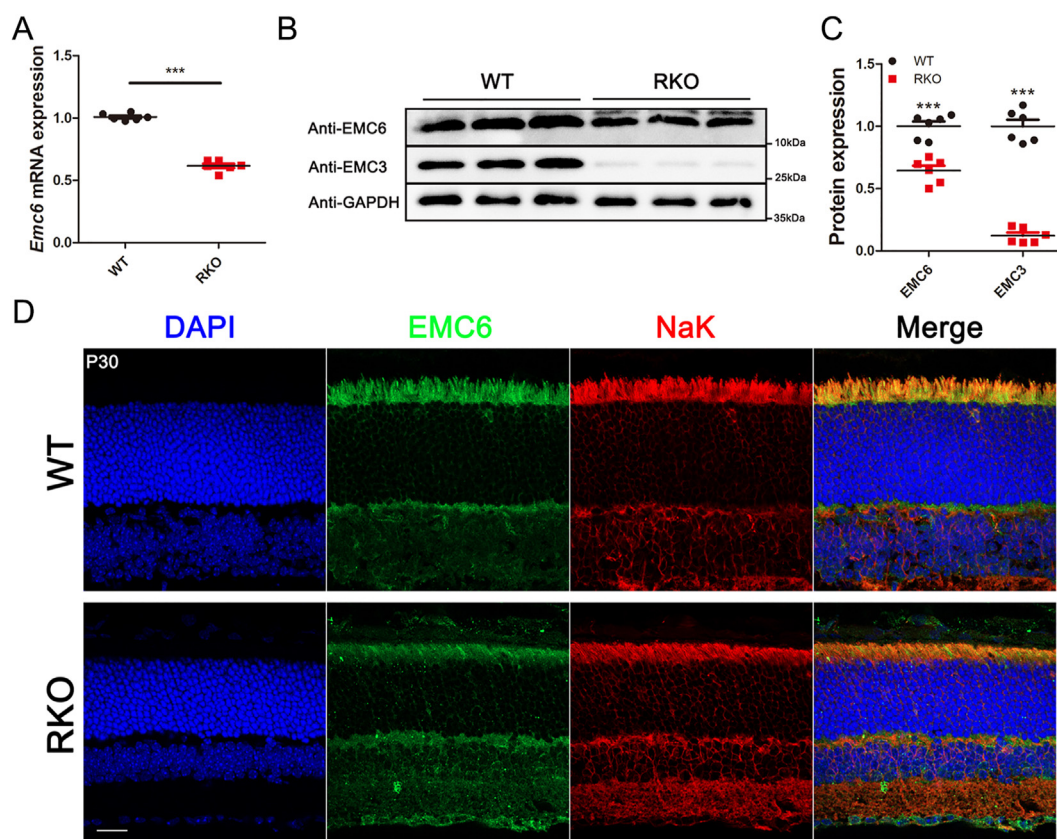


Figure 1 Generation of rod photoreceptor-specific *Emc6*-deleted mice. **(A)** RT-qPCR analysis revealed the expression of *Emc6* was decreased to 62% in RKO retinas. $n = 6$ for both WT and RKO. **(B, C)** Western blotting analysis of EMC6 and EMC3 protein expression in retinas of WT and RKO mice. GAPDH was used as an endogenous control. Relative protein band density was calculated by ImageJ. $n = 6$ for both WT and RKO. **(D)** Immunohistochemistry staining of retinas was labeled with EMC6 antibody (green) and NaK ATPase antibody (red). Cell nuclei were counterstained with DAPI (blue). Scale bars = 20 μm . Data were expressed as mean \pm SEM. Significance was calculated by a two-tailed Student's *t*-test. *** $P < 0.001$.

age. Retinas from each animal were harvested and immediately frozen. The samples were sent to JingJie Corporation (Hangzhou, Zhejiang, China) for LC-MS/MS Analysis. Differential protein expression screening was performed using a change in differential expression of more than 1.2 as the threshold for significant up-regulation and less than 1/1.2 as the threshold for significant down-regulation, with a *P* value less than 0.05.

Statistical analysis

Statistical significance was determined by a paired or unpaired Student's *t*-test with the GraphPad Prism6 Software. Quantitative data are shown as the mean \pm standard error of the mean (SEM). *P* values < 0.05 were considered statistically significant.

Results

Generation of *Emc6* conditional knockout mice

Previous studies have reported severe photoreceptor cell death in *emc6*^{N10} mutant flies and rhodopsin

mislocalization in rod photoreceptors of EMC3-deficient mice.²² To investigate the function of *Emc6* in mammalian photoreceptor cells and the detailed mechanism that affected the localization of rhodopsin, we generated RKO mice by crossing *Emc6* floxed mice with Rod-Cre mice (Fig. S1A). In addition, an *Emc6* cone knockout line was constructed using Cone-Cre mice (named CKO mice) (Fig. S1B). The genotypes of the offspring were determined by PCR (Fig. S1C, D).

We validated the knockdown efficiency of *Emc6* in rod cells of RKO mice. We harvested mRNA from the retinas of RKO mice and detected reduced expression of *Emc6* at the RNA level (Fig. 1A). Retinal protein extract of RKO mice was examined by western blotting analysis (Fig. 1B). The expression level of EMC6 was reduced to 63% in RKO mice compared with WT mice (Fig. 1B, C). In addition, we also detected reduced protein expression levels of EMC3, another EMC complex member, in RKO mice (Fig. 1B, C). This was in accordance with previous reports that almost all EMC subunits were lost in EMC6 knockdown.²⁹ Immunohistochemistry staining further confirmed that EMC6 was only present in cone photoreceptors in RKO mice (Fig. 1D). Detailed information on the study design is listed in Figure S2.

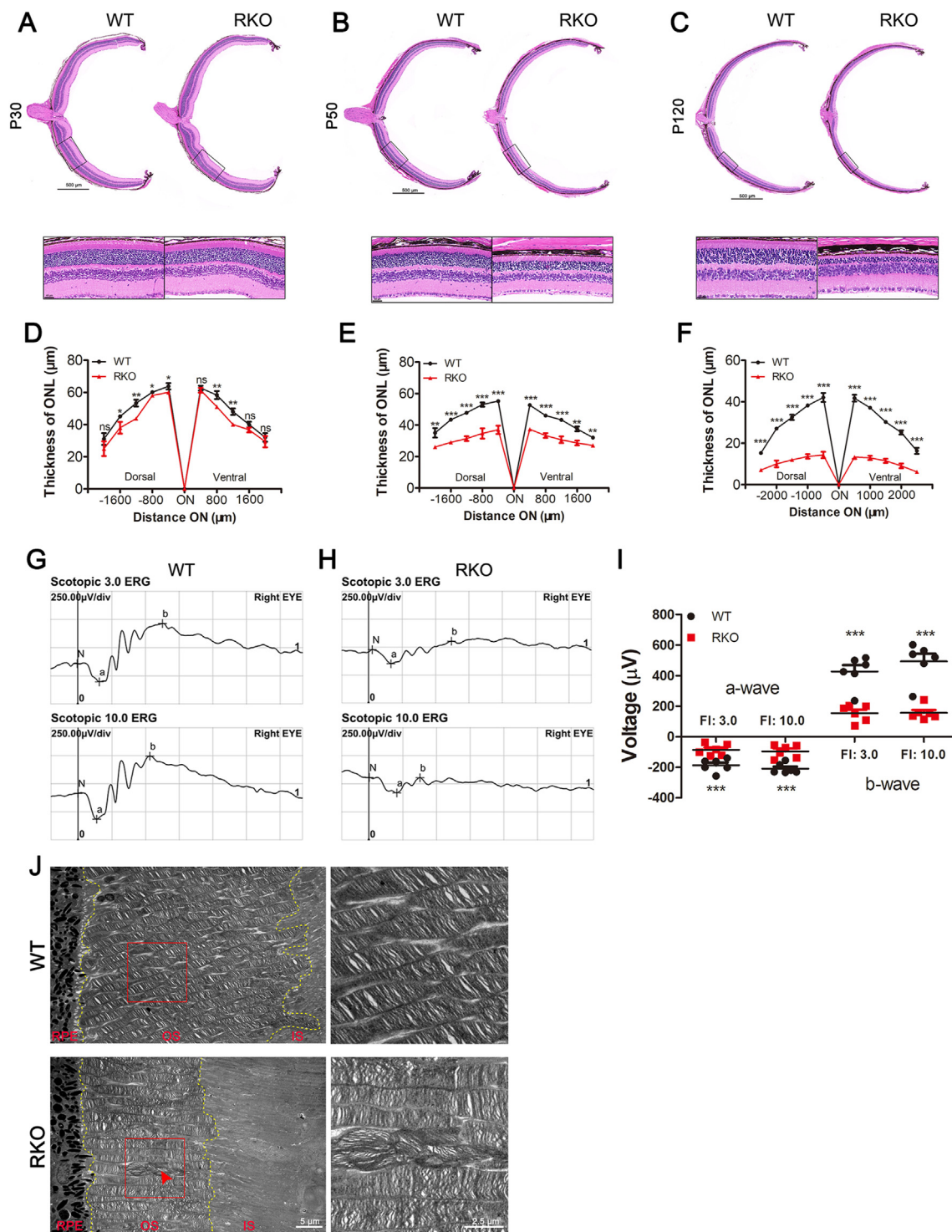


Figure 2 Progressive degeneration and impaired function in *Emc6* RKO mice. (A–C) Paraffin sections of the WT and RKO mouse retinas at the age of 30, 50, and 120 days were stained with H&E. Scale bars were 500 μm (upper panels) and 40 μm (lower panels). (D–F) Quantitative assessment of the ONL thickness in WT and RKO mouse retinas. $n = 6$ for both WT and RKO. (G, H) Representative ERG traces of WT and RKO mouse retinas at the age of 50 days under scotopic conditions at flash intensities of 3.0 and 10.0 $\text{cd}\cdot\text{s}/\text{m}^2$. $n = 6$ for both WT and RKO. (I) Statistical analysis of the a-waves and b-waves amplitudes under flash intensities of 3.0 and 10.0 $\text{cd}\cdot\text{s}/\text{m}^2$. (J) Transmission electron micrograph analysis of rod photoreceptors OS in WT and RKO mice at the age of 30 days. Red arrows represent the disorganized membrane disc of rod photoreceptors. Scale bars = 5 μm . Data were expressed as mean \pm SEM. Significance was calculated by a two-tailed Student's *t*-test. * $P < 0.05$, ** $P < 0.01$, *** $P < 0.001$; ns, not significant.

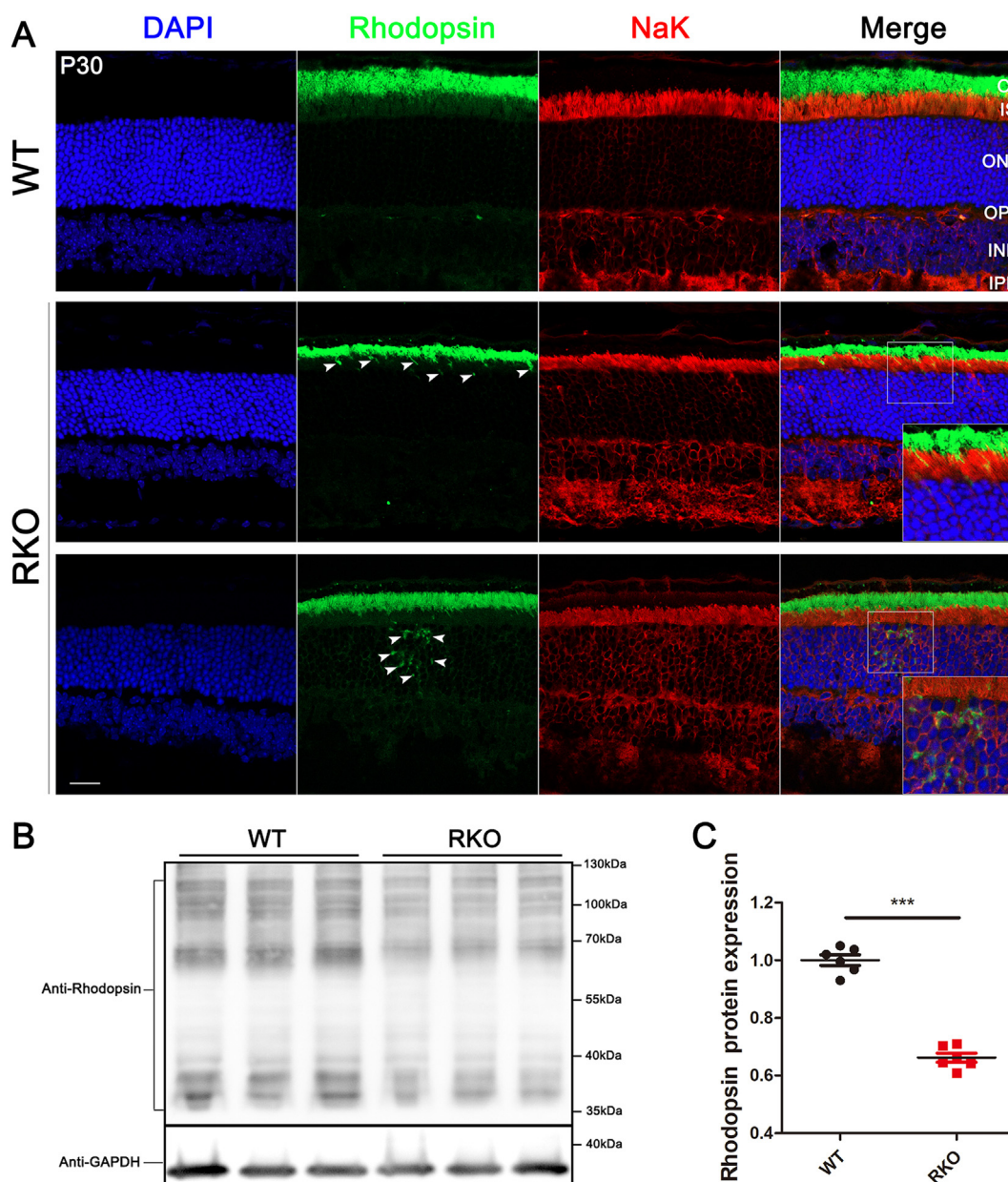


Figure 3 Mislocalization and reduced expression of rhodopsin protein in *Emc6* RKO retinas. (A) Immunohistochemistry staining analysis of WT and RKO mouse retinas at the age of 30 days. OS were labeled with Rhodopsin antibody (green) and IS were labeled with NaK ATPase antibody (red). Cell nuclei were counterstained with DAPI (blue). White arrows represent mislocalized Rhodopsin. Scale bars = 20 μ m. (B, C) Western blotting analysis of rhodopsin protein expression in retinas of WT and RKO mice. GAPDH was used as an endogenous control. Relative protein band density was calculated by ImageJ. $n = 6$ for both WT and RKO. Data were expressed as mean \pm SEM. Significance was calculated by a two-tailed Student's *t*-test. *** $P < 0.001$.

Emc6 is critical to rod photoreceptors' survival and retinal function

To assess the retina's phenotype caused by *Emc6* deletion, H&E staining of retina sections was performed on postnatal days 30, 50, and 120 (P30, P50, and P120). Quantitative analysis of the ONL thickness in WT and RKO retinas at P30 revealed that the ONL in the peripheral area in the WT mice began to become thinner compared with RKO mice (Fig. 2A, D). At P50, the ONL thickness of RKO mice was reduced by approximately 40% of WT mice (Fig. 2B, E). At P120, the

ONL was reduced to 3–4 cells per row in RKO mice compared with 10–11 cells per row in WT mice and only 30% of ONL remained in RKO mice compared to WT mice (Fig. 2C, F).

We further utilized scotopic ERG to evaluate the retinal function at P50. In the scotopic 3.0 and 10.0 response tests, both a-wave and b-wave amplitudes were significantly lower in RKO mice (Fig. 2G, H). The mean amplitudes of both a-wave and b-wave in RKO mice were reduced by approximately 60% (Fig. 2I), indicating impaired rod photoreceptor cell function. Compared with WT mice, the

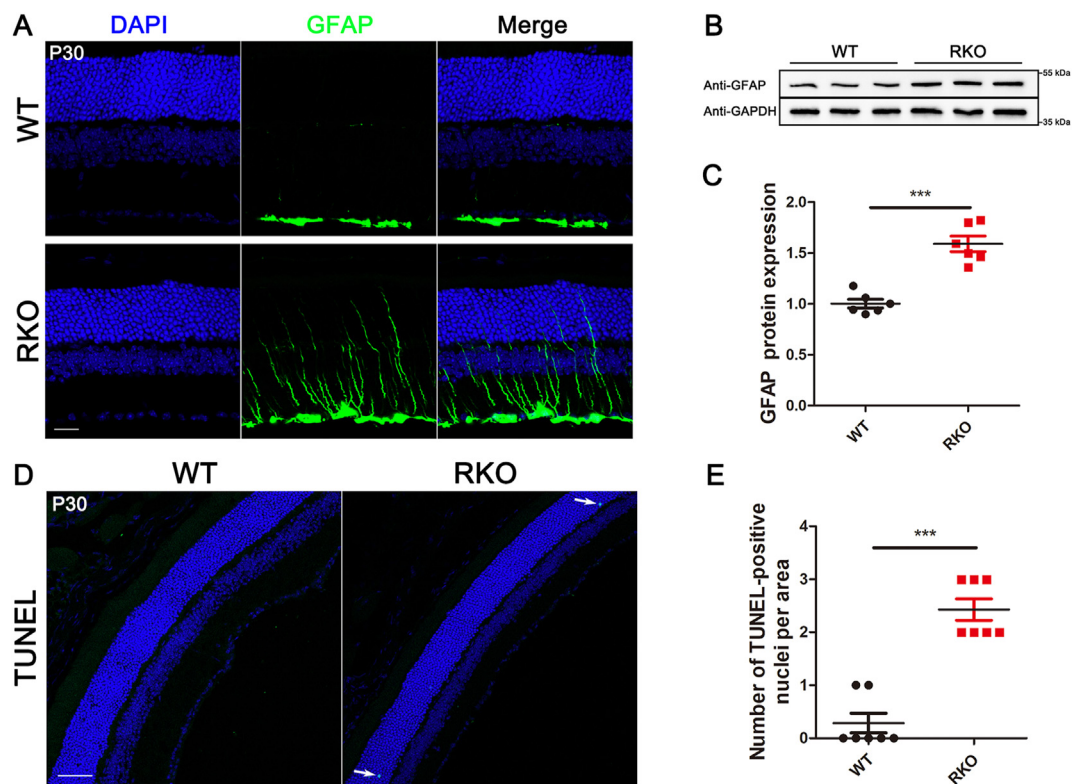


Figure 4 Astrogliosis and apoptotic cell death occur in the retina of *Emc6* RKO mice. (A) WT and RKO mouse retinas were immunostained with GFAP antibody (green) and counter-stained with DAPI (blue). Scale bars = 20 μ m. (B, C) Western blotting analysis of GFAP protein expression in retinas of WT and RKO mice at the age of 30 days. GAPDH was used as an endogenous control. Relative protein band density was calculated by ImageJ. $n = 6$ for both WT and RKO. (D, E) TUNEL assays in 30 days old WT and RKO mice. White arrows represent TUNEL-positive cells. Scale bars = 50 μ m. $n = 7$ for both WT and RKO. Data were expressed as mean \pm SEM. Significance was calculated by a two-tailed Student's *t*-test. ** $P < 0.01$, *** $P < 0.001$.

OS of RKO was significantly shortened and partially disorganized, as revealed by TEM analysis (Fig. 2J).

Mislocalization and gradual reduction of rhodopsin in RKO mice

Rhodopsin, as a major component of the OS of photoreceptors, is essential for normal visual function.^{30,31} To assess the consequences of *Emc6* knockout in mammals on the synthesis and transport of rhodopsin, we perform immunostaining on retinal cryosections from WT and RKO mice. Mislocalized rhodopsin protein was observed in P30 RKO mice, in parallel with the shortening of photoreceptor OS (Fig. 3A). We further verified rhodopsin protein expression by immunoblotting and revealed that rhodopsin protein expression was reduced by approximately 35% in RKO mice compared to WT mice (Fig. 3B, C). In addition, we examined the retinas of P21 mice and did not find shortened OS and mislocalization of rhodopsin in RKO mice (Fig. S3A). Immunostaining of retinal cryosections from older mice revealed that rhodopsin protein was barely expressed due to severe degeneration of the photoreceptor OS in P50 and P120 RKO mice (Fig. S3B, C). These results indicated that deletion of *Emc6* caused mislocalization of

rhodopsin protein and progressive degeneration of photoreceptor OS.

Increased gliosis and apoptosis in RKO mice

Mislocalized rhodopsin protein has been shown cytotoxic and triggers apoptotic cell death.^{32,33} We further explored the apoptosis in the retinas of P30 RKO mice. Astrocytes as normally neuroprotective were activated and characterized by reactive astrogliosis in pathological conditions.^{34,35} Reactive astrogliosis is a common symptom of retinal damage, so we stained retinal cryosections with glial fibrillary acidic protein (GFAP) antibody, which could reflect astrogliosis. In the retinas of WT mice, the fluorescent signal of GFAP was observed only in the ganglion cell layer (Fig. 4A). In contrast, in addition to the ganglion cell layer, the fluorescent signal of GFAP was also evident in the ONL, outer plexiform layer, inner nuclear layer, and the inner plexiform layer of the retinas in RKO mice (Fig. 4A). Further immunoblotting experiment confirmed an approximately 1.6-fold increase in GFAP expression in the retinas of RKO mice (Fig. 4B, C), indicating indeed pathological damage in RKO mice. TUNEL assay revealed apoptosis in the retinas of P30 RKO mice (Fig. 4D, E). TUNEL-labeled nuclei were mostly positioned in the ONL layer, indicating that

photoreceptor cells of RKO mice were undergoing apoptosis (Fig. 4D).

Depletion of *Emc6* results in cone photoreceptor defects in CKO mice

With the constructed CKO mice we analyzed the effect of EMC6 deficiency on cone cells playing a key role in color recognition. To examine the pathological changes of cones in CKO mice, retinas from P60 mice were coimmunostained with an L/M-opsin antibody and Alexa Fluor-594-conjugated PNA (which marks the cone matrix sheaths associated with all three types of cones). Immunostaining of retinal cryosections revealed reduced cone cells (Fig. 5A). Next, we quantified the number of cones in the dorsal retina of WT and CKO mice by immunostaining of whole-mount retina. As expected, a drastic reduction in the number of cone cells was observed in the CKO retina, consistent with the immunolabeling results of retinal cryosections (Fig. 5B, C). In addition, examination of higher-magnification images with retina cross-sections discovered numerous cells with mislocalized L/M-opsin (Fig. 5B, D). A similar pattern of rhodopsin mislocalization observed in RKO mice was considered, and we believe that a deficiency in protein transport to the OS caused by EMC6 deletion underlies the degeneration of retinal photoreceptors.

Emc6 deficiency impaired rod photoreceptor cilia

In order to investigate the molecular mechanisms leading to the mislocalization of rhodopsin protein, we conducted a proteomics analysis of retinas in 4-week-old RKO mice and littermate controls. Proteomics data analysis identified 49 proteins down-regulated and 46 proteins up-regulated (Fig. 6A). A large number of proteins related to ciliary development or maturation were down-regulated in RKO retinas (Fig. 6B). Multi-transmembrane proteins of particularly anoctamin-2 (ANO2) and transmembrane protein 67 (TMEM67) were discovered to be significantly down-regulated as illustrated in the volcano plot (Fig. 6C). ANO2 acted as a calcium-activated chloride channel and mediated signal amplification in olfactory sensory cilia.^{36,37} A previous study reported that chloride transport by ANO1 was required for the genesis or maintenance of primary cilia.³⁸ TMEM67 (also named MKS3) is mainly localized to the TZ of primary cilia and membranes covering the axoneme of the primary cilia.^{39,40} TMEM67, an essential component of ciliogenesis, is involved in the migration of centrosomes to the apical cell surface during early ciliogenesis. In the retina, TMEM67 has been reported to be critical for the maturation and maintenance of OS and transport of phototransduction molecules.^{41–43} Down-regulation of ANO2 and TMEM67 protein expression levels

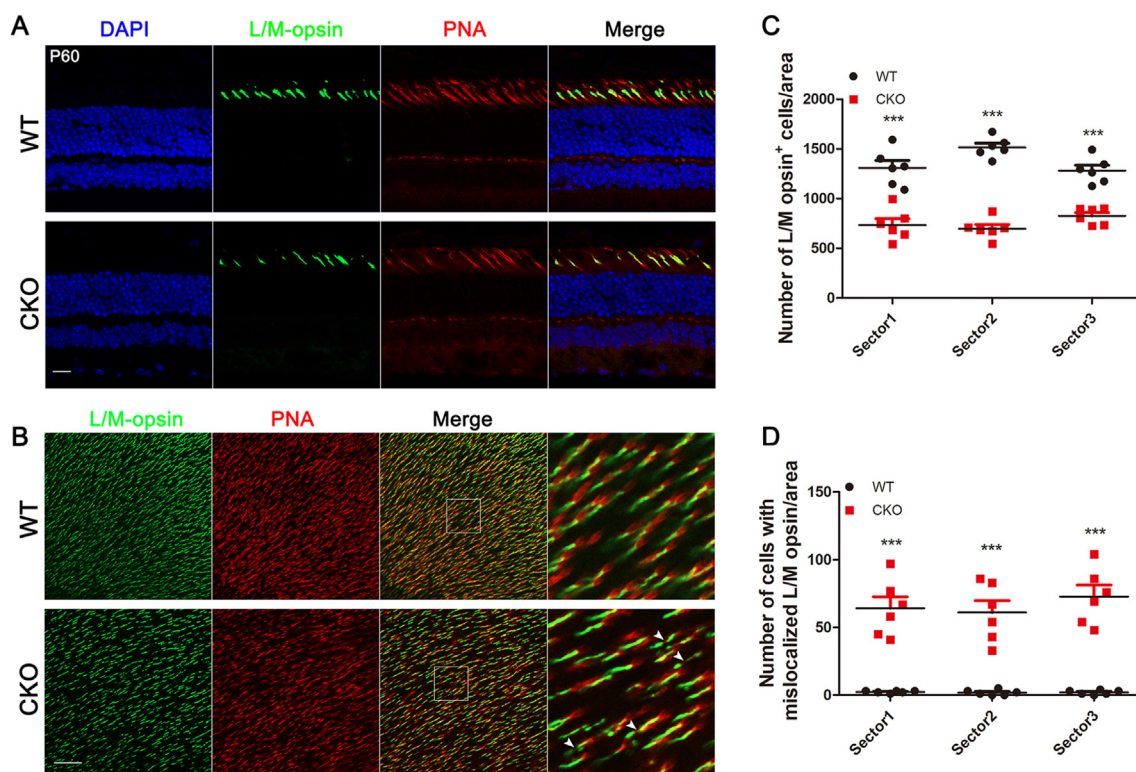


Figure 5 EMC6 depletion in cone cells leads to cone photoreceptor defects. (A) Retinal cryosections from P60 mice were labeled with the cone markers PNA and L/M-opsin. DAPI was used to counterstain the nuclei. Scale bars = 20 μm . (B) Immunostaining of flat-mount retinas from P60 control and CKO mice for L/M-opsin and PNA markers revealed cone cell reduction in CKO retinas. Scale bars = 50 μm . White arrowheads indicate mislocalized L/M-opsin in the cone cells. (C) The number of L/M-opsin-marked cones per field in the three sectors of WT and CKO retinas ($n = 6$). (D) The number of L/M-opsin-mislocalized cones per field in the three sectors of WT and CKO retinas ($n = 6$). Data were expressed as mean \pm SEM. Significance was calculated by a two-tailed Student's t -test. *** $P < 0.001$.

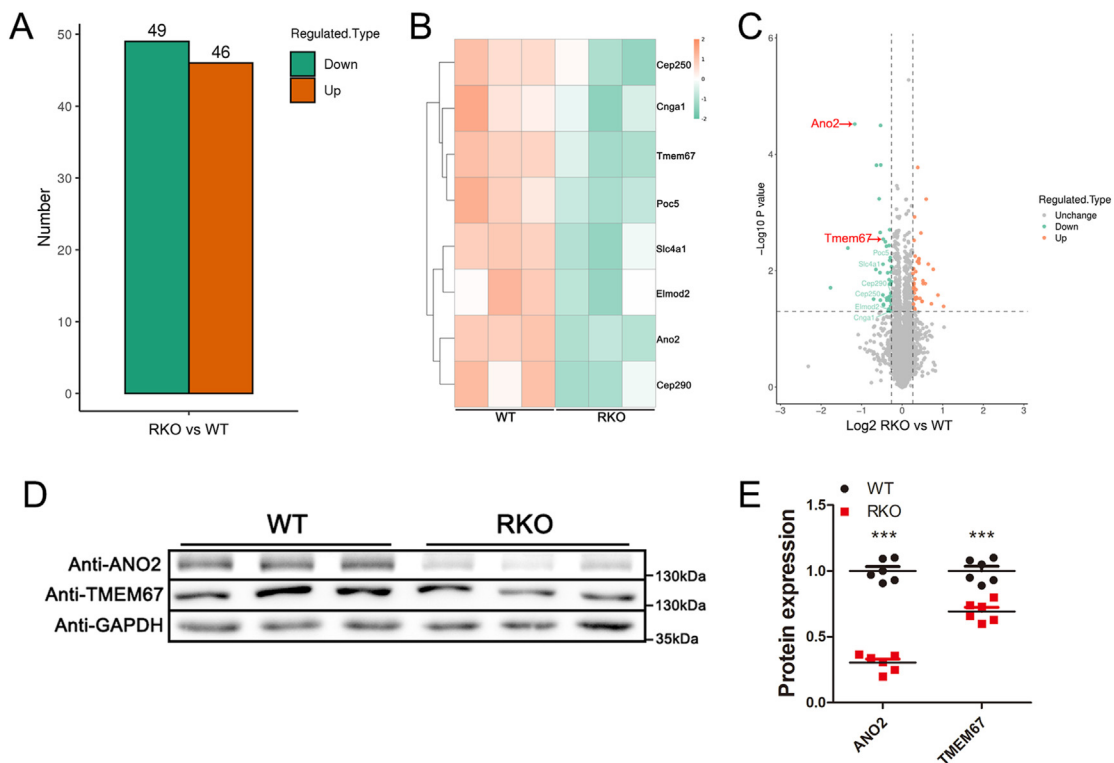


Figure 6 EMC6 was intimately interrelated with cilium-related proteins. (A) Statistical graphics of differentially expressed proteins in the RKO mouse retinas compared with WT. (B) The heatmap of the expression fold changes of several cilium-related proteins in RKO mouse retinas compared with WT as determined by proteomics analysis. (C) The volcano plot of differentially expressed proteins in the RKO mouse retinas compared with WT. Proteins of ANO2 and TMEM67 were displayed. (D, E) Western blotting analysis of ANO2 and TMEM67 protein expression in retinas of WT and RKO mice at the age of 28 days. GAPDH was used as an endogenous control. Relative protein band density was calculated by ImageJ. $n = 6$ for both WT and RKO. Data were expressed as mean \pm SEM. Significance was calculated by a two-tailed Student's t -test. $**P < 0.01$, $***P < 0.001$.

was confirmed by immunoblotting in RKO mice (Fig. 6D, E). However, the RT-qPCR results showed that the mRNA expression of cilium-related proteins was not significantly reduced (Fig. S4). This indicated that the loss of EMC6 does not affect the transcription of cilium-related genes.

Immunostained retinal cryosections show that ANO2 is mainly localized to the outer plexiform layer and IS, while TMEM67 is localized to IS in the murine retina (Fig. S5A, B). Previous research had indicated that ANO2 was localized on the cilia of olfactory sensory neurons in mice.³⁶ We further discovered by high magnification photos that ANO2 was localized in a broad area of the photoreceptor cilium, including the BB and CC, which is unprecedented (Fig. 7A). TMEM67 was also expressed in CC (Fig. 7B).

Immunostaining of the rod photoreceptor cilium with acetylated α -tubulin which was a characterized marker of ciliary axoneme⁴⁴ and γ -tubulin revealed that both the length and the number of rod photoreceptor cilia decreased in RKO mice (Fig. 7C, E, F). Immunostaining for centrin, a marker of the TZ of cilium,⁴⁵ demonstrated that the rod photoreceptor cilia were also defective (Fig. 7D, G, H). To further confirm these results, we explored the photoreceptor longitudinal sections with TEM. Consistent with the immunostaining data, TEM indicated that the CC length of RKO mice became significantly shorter compared with WT mice (Fig. 7I). However, the "9 + 0" microtubule structure of rod photoreceptor

cilium did not appear abnormal (Fig. S6). Taken together, these data suggest that loss of *Emc6* led to reduced levels of cilium-associated proteins and defective cilia.

The transport of membrane disc proteins was impaired in RKO mice

We subsequently investigated a variety of OS membrane proteins involved in the phototransduction process. In RKO mice, mislocalized GNAT1 and GNB1 were observed in IS (Fig. 8A, B), and the expression level of GNAT1 was reduced while no obvious change in GNB1 expression was observed in RKO mice (Fig. 8E, F). Immunostaining of phosphodiesterase 6B (PDE6B) and phosphodiesterase 6G (PDE6G) demonstrated that the transport of PDE from IS to OS is compromised in RKO mice (Fig. 8C, D). The expression of PDE6B was significantly reduced in RKO mice (Fig. 8E, F). These data implicated that defective cilia led to the mislocalization of membrane disc proteins in the absence of EMC6.

ANO2 and TMEM67 expression was reduced prior to OS degeneration in RKO mice

To further examine the role of ANO2 and TMEM67 in the retinal degeneration process of RKO mice, we extracted

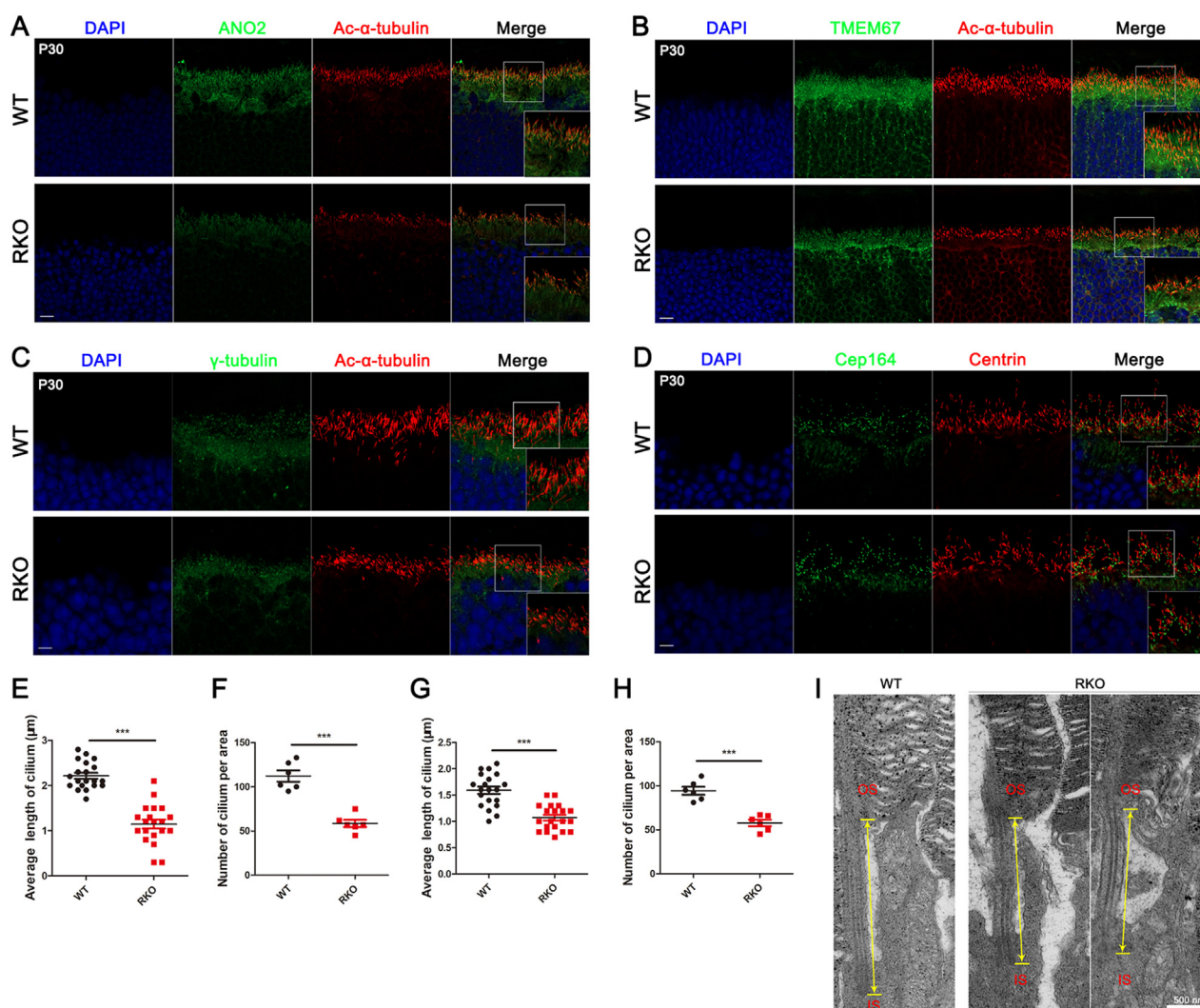


Figure 7 Rod photoreceptor cilia were abnormal in *Emc6* RKO mice. (A, B) Retinal cryosections were labeled with ANO2 antibody (A) (green), TMEM67 antibody (B) (green), and Ace- α -tubulin antibody (red). Cell nuclei were counterstained with DAPI (blue). Scale bars = 10 μ m. (C, E, F) Immunohistochemistry images (C) and quantification of the length (E) and number (F) of cilia in rod photoreceptors from WT and RKO mice. Retinal cryosections were stained with γ -tubulin antibody (green) and Ace- α -tubulin antibody (red). Cell nuclei were counterstained with DAPI (blue). Scale bars = 10 μ m. (D, G, H) Immunohistochemistry images (D) and quantification of the TZ length (G) and number (H) of cilia in rod photoreceptors from WT and RKO mice. Retinal cryosections were stained with Cep164 antibody (green) and Centrin antibody (red). Cell nuclei were counterstained with DAPI (blue). Scale bars = 10 μ m. (I) TEM images of the longitudinal sections of rod photoreceptor cilium in WT and RKO mice. Scale bars = 500 nm. Data were expressed as mean \pm SEM. Significance was calculated by a two-tailed Student's *t*-test. ****P* < 0.001.

total retinal proteins from P21 WT and RKO mice. The results showed that ANO2 and TMEM67 were reduced by 67% and 58%, respectively (Fig. 9A, B), which is generally consistent with the results of P30 mice (Fig. 6D, E). Previous immunostaining results showed no shortening of OS and no mislocalization of rhodopsin in P21 RKO mice (Fig. 53A). Rhodopsin expression in the retinas of P21 RKO mice was not significantly decreased (Fig. 9A, B), unlike the retinas of P30 RKO mice in which rhodopsin was significantly reduced (Fig. 3B, C). In addition, the expression of the phototransduction proteins GNAT1, GNB1, PDE6B, and PDE6G did not display any variation in P21 RKO mice (Fig. 9A, B). There was also a significant decrease in ANO2 and TMEM67 by immunostaining study in P21 RKO mice (Fig. 9C, D). Further research found that the rod photoreceptor cilia began to

shorten, but the number did not change significantly (Fig. 9E–G). In short, these results demonstrated that the expression changes of ANO2 and TMEM67 precede OS degeneration. Therefore, the essential reason for the mislocalization of rhodopsin and phototransduction proteins is most likely to be a result of reduced expression of ANO2 and TMEM67, leading to abnormal rod photoreceptor cilia and blocking the normal transport of proteins from the IS to OS.

Discussion

In the present study, we investigated the roles of EMC6 in the retina by generating rod-specific *Emc6* conditional knockout (RKO) mice, in which EMC6 was specifically

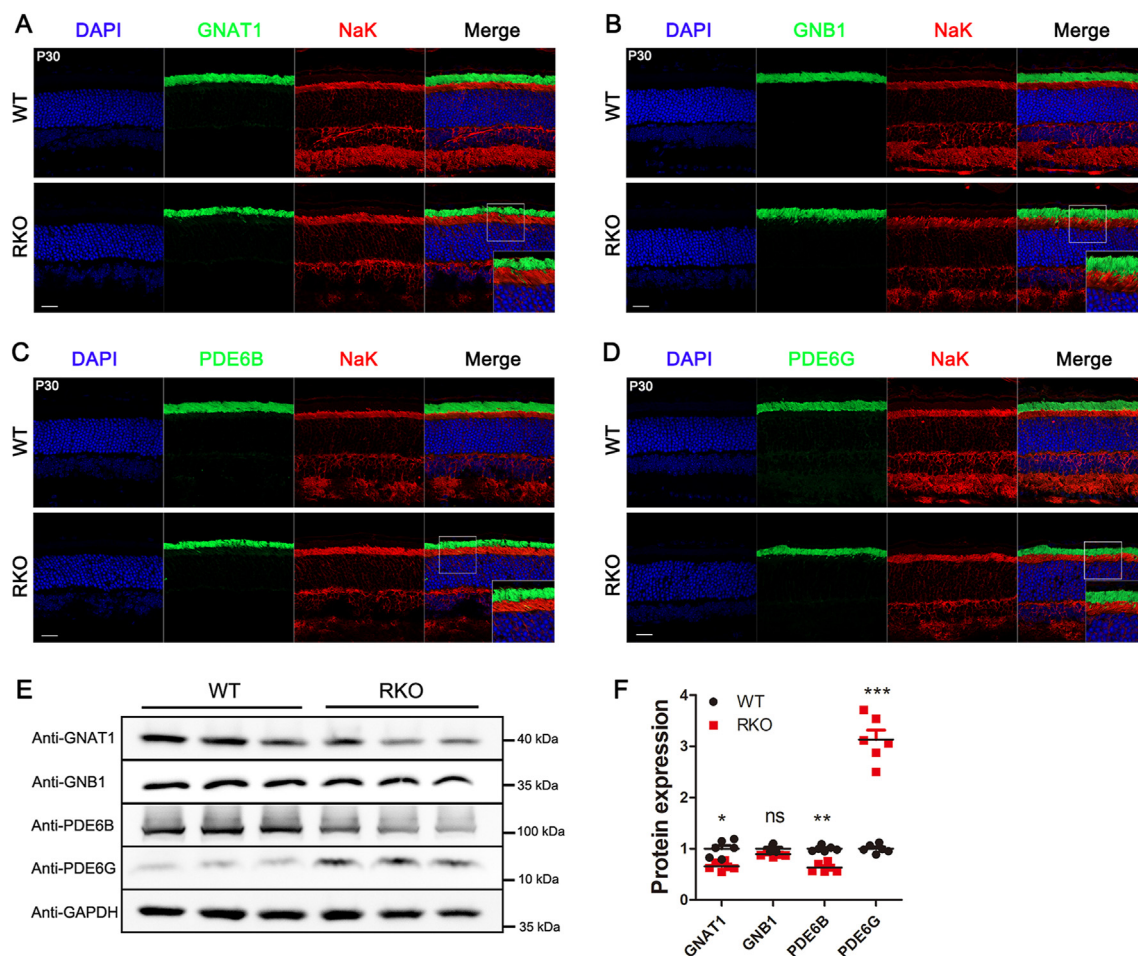


Figure 8 Mislocalization of membrane disc proteins in *Emc6* RKO mice. (A–D) Retinal cryosections were labeled with NaK ATPase antibody (red) located in IS. GNAT1 (A), GNB1 (B), PDE6B (C), and PDE6G (D) antibodies were used to stain retinal cryosections, respectively. Cell nuclei were counterstained with DAPI (blue). Scale bars = 20 μ m. (E, F) Immunoblotting (E) and quantification (F) analysis of membrane disc proteins (GNAT1, GNB1, PDE6B, and PDE6G) in retinas of 30-day-old WT and RKO mice. GAPDH was used as an endogenous control. Relative protein band density was calculated by ImageJ. $n = 6$ for both WT and RKO. Data were expressed as mean \pm SEM. Significance was calculated by a two-tailed Student's *t*-test. * $P < 0.05$, ** $P < 0.01$, *** $P < 0.001$; ns, not significant.

deleted from the rod photoreceptor cells. RKO mice displayed early onset retinal degeneration with retinal functional impairment and progressive death of photoreceptor cells. This phenotype is due to the mislocalization of rhodopsin and some other membrane disc proteins, suggesting that EMC6 plays a critical role in the transport of membrane disc proteins in photoreceptor cells. In addition, deficiency of *Emc6* leads to down-regulation of cilium-related protein ANO2 and TMEM67 expression, blockage of cilium development, subsequently disruption of membrane disc protein transport, and ultimately photoreceptor cell degeneration. In conclusion, our data demonstrate that EMC6 plays a pivotal function in the synthesis and transport of rhodopsin and other membrane disc proteins.

EMC is critical in the insertion of membrane proteins into the lipid bilayer of ER.^{12–14} Several studies indicated that different EMC subunits have distinct functions.^{15,22–25,46} In a genome-wide genetic screen of *Caenorhabditis elegans* mutants, Richard et al isolated EMC6 and found that EMC6 is essential for acetylcholine receptor synthesis.²⁵ By the cell-

based functional screening platform, a novel gene (*Emc6*) associated with cell autophagy was identified.²⁴ EMC1 plays an essential role in the SV40 ER to cytoplasmic lysosomal membrane transport, which prevents premature breakdown of envelope-free viruses.¹⁵ *Emc10* was identified as a vascular growth factor by a bioinformatic secretome analysis in bone marrow cells.⁴⁶ These studies indicated that each subunit of EMC may have distinct functions. Furthermore, EMC6 is localized in the ER. However, when EMC5 is absent, EMC6 is concentrated in intracellular vesicles.²² This implies that EMC6 may perform independent functions outside the ER, which is also consistent with studies linking EMC6 to acetylcholine receptor synthesis and autophagy. Only three subunits of EMC (EMC3, EMC5, and EMC6) were enriched by genome-wide screening of *Drosophila* mutants with reduced rhodopsin expression.²² This is probably because EMC3, EMC5, and EMC6 are at the core of the three-dimensional structure of the EMC.^{47,48} As a result of the close spatial association between EMC3 and EMC6, EMC3 expression is reduced in the retinas of *Emc6* RKO mice

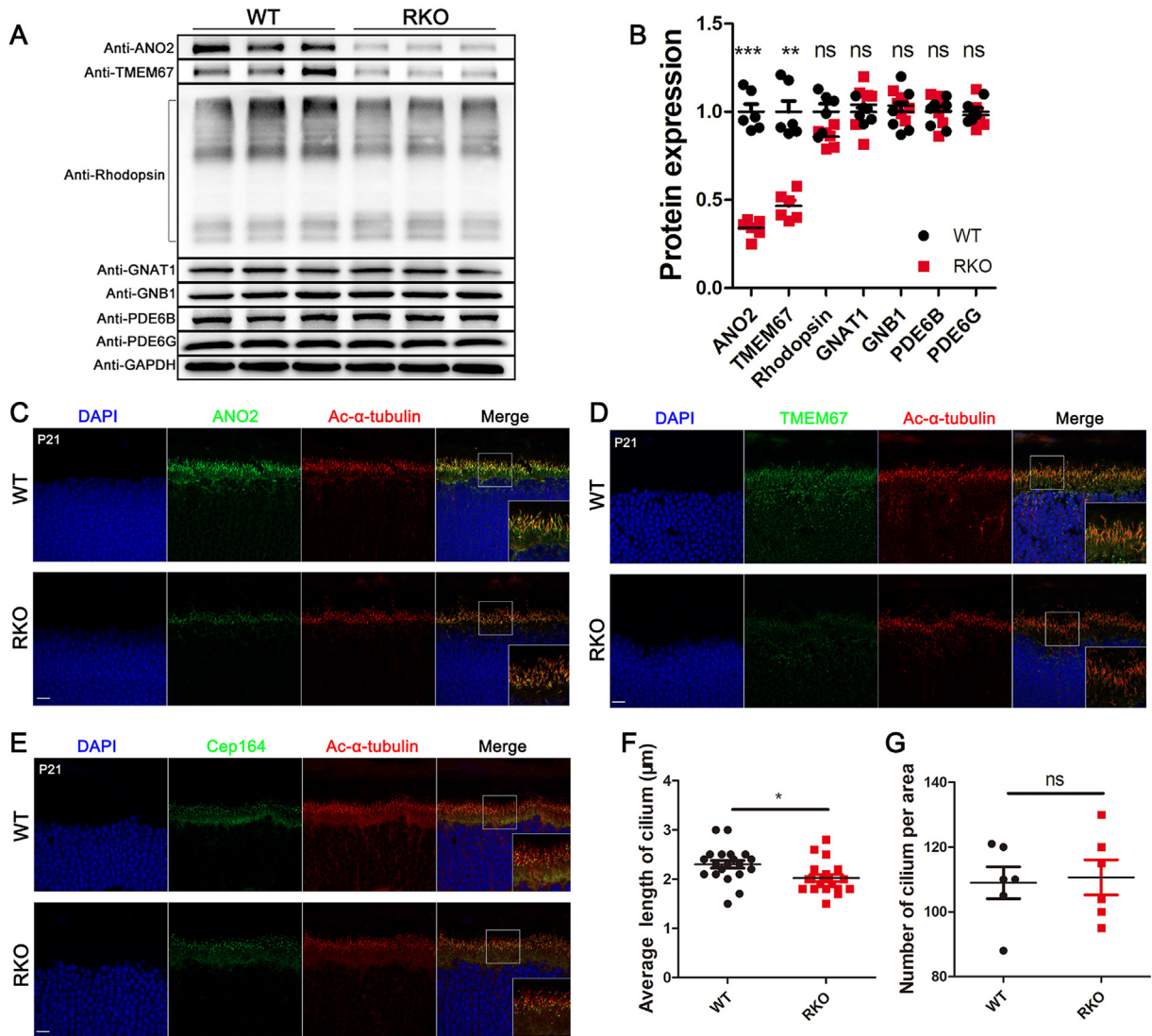


Figure 9 ANO2 and TMEM67 protein expression decreased in P21 *EMC6* RKO mice. (A, B) Western blotting analysis of ANO2, TMEM67, Rhodopsin, GNAT1, GNB1, PDE6B, and PDE6G protein expression in retinas of WT and RKO mice. GAPDH was used as an endogenous control. Relative protein band density was calculated by ImageJ. $n = 6$ for both WT and RKO. (C, D) Retinal cryosections were labeled with ANO2 antibody (C) (green), TMEM67 antibody (D) (green), and Ace- α -tubulin antibody (red). Cell nuclei were counterstained with DAPI (blue). Scale bars = 10 μ m. (E–G) Immunohistochemistry images (E) and quantification of the length (F) and number (G) of cilia in rod photoreceptors from WT and RKO mice. Retinal cryosections were stained with Cep164 antibody (green) and Ace- α -tubulin antibody (red). Cell nuclei were counterstained with DAPI (blue). Scale bars = 10 μ m. Data were expressed as mean \pm SEM. Significance was calculated by a two-tailed Student's *t*-test. $^{**}P < 0.01$.

(Fig. 1B, C). No visible defects were observed in *Drosophila* mutants with *emc7* and *emc10* deletion, which suggested that these two subunits were not essential for the function of other subunits.²²

Emc6 deficiency resulted in diminished expression levels of cilia-associated proteins ANO2 and TMEM67. This is attributed to the fact that both ANO2 and TMEM67 are multi-transmembrane proteins, and the absence of EMC6 prevented ANO2 and TMEM67 from forming a TMD structural domain, resulting in the inability to enter the ER for further processing and the eventual degradation of immature ANO2 and TMEM67. More recently, a proteomic analysis using EMC KD cells identified a series of potential EMC client proteins,

including ANO6 (TMEM16F) and ANO10 (TMEM16K).^{49,50} This supported the notion that ANO2 serves as a client protein for EMC. In olfactory signal transduction, ANO2 was recognized as an essential chloride channel in olfactory sensory neurons cilia.³⁷ Ion channels were abundant in the retinas and played vital roles in the signal transmission process. There were two main types of ion channels in rod photoreceptors, including ion channels located at synaptic terminals and cyclic nucleotide-gated ion channels located at OS. Mutations in several ion channels were reported to be associated with autosomal recessive retinitis pigmentosa.^{51–55} We identified for the first time that the chloride channel protein ANO2, which was regulated by

calcium ions, was expressed in rod photoreceptor cilia (Fig. 7A), and rod photoreceptor cilia were severely damaged in *Emc6* RKO mice (Fig. 7C–H). Previously, it had been demonstrated that ANO1 was crucial for primary cilia.³⁸ Consequently, severe impairment of rod photoreceptor cilia in RKO mice may be partly caused by the blockage of ANO2-mediated chloride transport in rod photoreceptor cilia. TMEM67 has been proven to be expressed in rod photoreceptor cilia and to be involved in molecular and protein transport.^{42,43} Decreased expression of TMEM67, an important component of cilia, impairs rod photoreceptor cilium formation and maintenance, resulting in impaired molecular and protein transport from IS to OS.

The OS of rod photoreceptors was generally regarded as a highly modified and specialized primary cilium.^{56,57} The structure of the rod photoreceptor cilium consisted of an axoneme of nine triplet microtubule doublets extending from the BB.⁵⁸ Due to the high-level protein requirement of OS, the transport along the cilium was crucial for the survival and function of photoreceptors.^{9,10} Deficiency of *Emc6* resulted in disruption of cilia, which significantly decreased the efficiency of protein transport along the cilium and accumulation of various disc membrane proteins in the IS (Fig. 8). Failure to comply with the protein requirements of OS caused progressive degeneration and loss of function of rod photoreceptor cells.

During phototransduction, activated rhodopsin initiate transducin (GNAT1 and GNB1 in rod photoreceptors) that convert $G\alpha\beta\gamma$ -GDP to $G\alpha$ -GTP.^{59,60} Due to the relatively low level of GNB1 as transducin in rod photoreceptors (mainly GNAT1), we failed to detect significant changes in GNB1 protein expression (Fig. 8E, F). PDE is a tetrameric protein composed of two equally active catalytic subunits (α and β) and two identical γ subunits.^{61,62} Under the light, $G\alpha$ -GTP replaces PDE6G and binds to PDE $\alpha\beta$, catalyzing cGMP hydrolysis. We analyzed two factors regarding the high expression of PDE6G which was detected in RKO mice (Fig. 8E, F). It is because PDE is anchored to the membrane disc through the C-terminus of the two catalytic subunits,^{63,64} so PDE6G does not bind directly to the membrane disc and is not affected by the functional defect of EMC. On the other hand, because of blocked phototransduction activation in RKO mice, activated photoreceptors need to be restored to an inactivated state more rapidly. The rate-limiting step is PDE deactivation, a process that requires more PDE6G to enhance the GAP activity of transducin, facilitating the conversion of $G\alpha$ -GTP to $G\alpha\beta\gamma$ -GDP and deactivating PDE.^{65,66}

In conclusion, our study on the role of *Emc6* in the retina revealed that loss of *Emc6* led to early-onset retinal degeneration and mislocalization of rhodopsin and other membrane disc proteins. These data highlight the important roles of EMC6 in the synthesis and transport of rhodopsin in retinal photoreceptors.

Conflict of interests

All authors declare that there are no competing interests.

Funding

This study was supported by The National Natural Science Foundation of China (No. 82121003, 81970841, 82101160), the program of Science and Technology International Cooperation Project of Qinghai province (China) (No. 2022-HZ-814), the CAMS Innovation Fund for Medical Sciences (No. 2019-12M-5-032), Sichuan Intellectual Property Office (China) (No. 2022-ZS-0070), and the Department of Chengdu Science and Technology (Sichuan, China) (No. 2021-YF05-01316-SN). The funders had no role in the study design, data collection, and analysis, or manuscript preparation.

Acknowledgements

The authors would like to thank Chengdu LiLai Biotechnology Co., Ltd., for technical assistance with histology analysis.

Appendix A. Supplementary data

Supplementary data to this article can be found online at <https://doi.org/10.1016/j.gendis.2023.03.033>.

References

- Daiger SP, Sullivan LS, Bowne SJ. Genes and mutations causing retinitis pigmentosa. *Clin Genet.* 2013;84(2):132–141.
- Neveling K, Collin RWJ, Gilissen C, et al. Next-generation genetic testing for retinitis pigmentosa. *Hum Mutat.* 2012;33(6):963–972.
- Hartong DT, Berson EL, Dryja TP. Retinitis pigmentosa. *Lancet.* 2006;368(9549):1795–1809.
- Sullivan LS, Bowne SJ, Birch DG, et al. Prevalence of disease-causing mutations in families with autosomal dominant retinitis pigmentosa: a screen of known genes in 200 families. *Invest Ophthalmol Vis Sci.* 2006;47(7):3052–3064.
- Verbakel SK, van Huet RAC, Boon CJF, et al. Non-syndromic retinitis pigmentosa. *Prog Retin Eye Res.* 2018;66:157–186.
- Nemet I, Ropelewski P, Imanishi Y. Rhodopsin trafficking and mistrafficking: signals, molecular components, and mechanisms. *Prog Mol Biol Transl Sci.* 2015;132:39–71.
- Mendes HF, van der Spuy J, Chapple JP, Cheetham ME. Mechanisms of cell death in rhodopsin retinitis pigmentosa: implications for therapy. *Trends Mol Med.* 2005;11(4):177–185.
- Xiong B, Bellen HJ. Rhodopsin homeostasis and retinal degeneration: lessons from the fly. *Trends Neurosci.* 2013;36(11):652–660.
- Young RW. The renewal of photoreceptor cell outer segments. *J Cell Biol.* 1967;33(1):61–72.
- Wolfrum U, Schmitt A. Rhodopsin transport in the membrane of the connecting cilium of mammalian photoreceptor cells. *Cell Motil Cytoskeleton.* 2000;46(2):95–107.
- Pearring JN, Salinas RY, Baker SA, Arshavsky VY. Protein sorting, targeting and trafficking in photoreceptor cells. *Prog Retin Eye Res.* 2013;36:24–51.

12. Jonikas MC, Collins SR, Denic V, et al. Comprehensive characterization of genes required for protein folding in the endoplasmic reticulum. *Science*. 2009;323(5922):1693–1697.
13. Guna A, Volkmar N, Christianson JC, Hegde RS. The ER membrane protein complex is a transmembrane domain insertase. *Science*. 2018;359(6374):470–473.
14. Chitwood PJ, Juszkwicz S, Guna A, Shao S, Hegde RS. EMC is required to initiate accurate membrane protein topogenesis. *Cell*. 2018;175(6):1507–1519.e16.
15. Bagchi P, Inoue T, Tsai B. EMC1-dependent stabilization drives membrane penetration of a partially destabilized non-enveloped virus. *Elife*. 2016;5:e21470.
16. Kawata K, Baba A, Shiota M, Wanibuchi H, Baba Y. ER membrane protein complex 1 interacts with STIM1 and regulates store-operated Ca^{2+} entry. *J Biochem*. 2021;170(4):483–488.
17. Marquez J, Criscione J, Charney RM, et al. Disrupted ER membrane protein complex-mediated topogenesis drives congenital neural crest defects. *J Clin Invest*. 2020;130(2):813–826.
18. Abu-Safieh L, Alrashed M, Anazi S, et al. Autozygome-guided exome sequencing in retinal dystrophy patients reveals pathogenic mutations and novel candidate disease genes. *Genome Res*. 2013;23(2):236–247.
19. Harel T, Yesil G, Bayram Y, et al. Monoallelic and biallelic variants in EMC1 identified in individuals with global developmental delay, hypotonia, scoliosis, and cerebellar atrophy. *Am J Hum Genet*. 2016;98(3):562–570.
20. Geetha TS, Lingappa L, Jain AR, et al. A novel splice variant in EMC1 is associated with cerebellar atrophy, visual impairment, psychomotor retardation with epilepsy. *Mol Genet Genomic Med*. 2018;6(2):282–287.
21. Cabet S, Lesca G, Labalme A, et al. Novel truncating and missense variants extending the spectrum of EMC1-related phenotypes, causing autism spectrum disorder, severe global developmental delay and visual impairment. *Eur J Med Genet*. 2020;63(6):103897.
22. Xiong L, Zhang L, Yang Y, et al. ER complex proteins are required for rhodopsin biosynthesis and photoreceptor survival in *Drosophila* and mice. *Cell Death Differ*. 2020;27(2):646–661.
23. Satoh T, Ohba A, Liu Z, Inagaki T, Satoh AK. dPob/EMC is essential for biosynthesis of rhodopsin and other multi-pass membrane proteins in *Drosophila* photoreceptors. *Elife*. 2015;4:e06306.
24. Li Y, Zhao Y, Hu J, et al. A novel ER-localized transmembrane protein, EMC6, interacts with RAB5A and regulates cell autophagy. *Autophagy*. 2013;9(2):150–163.
25. Richard M, Boulin T, Robert VJP, Richmond JE, Bessereau JL. Biosynthesis of ionotropic acetylcholine receptors requires the evolutionarily conserved ER membrane complex. *Proc Natl Acad Sci U S A*. 2013;110(11):E1055–E1063.
26. Shen X, Kan S, Hu J, et al. EMC6/TMEM93 suppresses glioblastoma proliferation by modulating autophagy. *Cell Death Dis*. 2016;7(1):e2043.
27. Tan JH, Cao RC, Zhou L, et al. EMC6 regulates acinar apoptosis via APAF₁ in acute and chronic pancreatitis. *Cell Death Dis*. 2020;11(11):966.
28. Li S, Chen D, Sauv e Y, McCandless J, Chen YJ, Chen CK. Rhodopsin-iCre transgenic mouse line for Cre-mediated rod-specific gene targeting. *Genesis*. 2005;41(2):73–80.
29. Volkmar N, Thezenas ML, Louie SM, et al. The ER membrane protein complex promotes biogenesis of sterol-related enzymes maintaining cholesterol homeostasis. *J Cell Sci*. 2019;132(2):jcs223453.
30. Lem J, Krasnoperova NV, Calvert PD, et al. Morphological, physiological, and biochemical changes in rhodopsin knockout mice. *Proc Natl Acad Sci U S A*. 1999;96(2):736–741.
31. Humphries MM, Rancourt D, Farrar GJ, et al. Retinopathy induced in mice by targeted disruption of the rhodopsin gene. *Nat Genet*. 1997;15(2):216–219.
32. Alloway PG, Howard L, Dolph PJ. The formation of stable rhodopsin-arrestin complexes induces apoptosis and photoreceptor cell degeneration. *Neuron*. 2000;28(1):129–138.
33. Zhang L, Sun Z, Zhao P, et al. Whole-exome sequencing revealed HKDC1 as a candidate gene associated with autosomal-recessive retinitis pigmentosa. *Hum Mol Genet*. 2018;27(23):4157–4168.
34. Dong Y, Benveniste EN. Immune function of astrocytes. *Glia*. 2001;36(2):180–190.
35. Sofroniew MV. Molecular dissection of reactive astrogliosis and glial scar formation. *Trends Neurosci*. 2009;32(12):638–647.
36. Stephan AB, Shum EY, Hirsh S, Cygnar KD, Reisert J, Zhao H. ANO₂ is the ciliary calcium-activated chloride channel that may mediate olfactory amplification. *Proc Natl Acad Sci U S A*. 2009;106(28):11776–11781.
37. Hengl T, Kaneko H, Dauner K, Vocke K, Frings S, M ohlen F. Molecular components of signal amplification in olfactory sensory cilia. *Proc Natl Acad Sci U S A*. 2010;107(13):6052–6057.
38. Ruppensburg CC, Hartzell HC. The Ca^{2+} -activated Cl⁻ channel ANO1/TMEM16A regulates primary ciliogenesis. *Mol Biol Cell*. 2014;25(11):1793–1807.
39. Dawe HR, Smith UM, Cullinane AR, et al. The Meckel-Gruber Syndrome proteins MKS1 and meckelin interact and are required for primary cilium formation. *Hum Mol Genet*. 2007;16(2):173–186.
40. Garcia-Gonzalo FR, Corbit KC, Sireerol-Piquer MS, et al. A transition zone complex regulates mammalian ciliogenesis and ciliary membrane composition. *Nat Genet*. 2011;43(8):776–784.
41. Tiwari S, Hudson S, Gattone 2nd VH, Miller C, Chernoff EAG, Belecky-Adams TL. Meckelin 3 is necessary for photoreceptor outer segment development in rat Meckel syndrome. *PLoS One*. 2013;8(3):e59306.
42. Collin GB, Won J, Hicks WL, Cook SA, Nishina PM, Naggert JK. Meckelin is necessary for photoreceptor intraciliary transport and outer segment morphogenesis. *Invest Ophthalmol Vis Sci*. 2012;53(2):967–974.
43. Leightner AC, Hommerding CJ, Peng Y, et al. The Meckel syndrome protein meckelin (TMEM67) is a key regulator of cilia function but is not required for tissue planar polarity. *Hum Mol Genet*. 2013;22(10):2024–2040.
44. L’Hernault SW, Rosenbaum JL. *Chlamydomonas* alpha-tubulin is posttranslationally modified by acetylation on the epsilon-amino group of a lysine. *Biochemistry*. 1985;24(2):473–478.
45. Wolfrum U. Centrin in the photoreceptor cells of mammalian retinae. *Cell Motil Cytoskeleton*. 1995;32(1):55–64.
46. Reboll MR, Korf-Klingebiel M, Klede S, et al. EMC10 (endoplasmic reticulum membrane protein complex subunit 10) is a bone marrow-derived angiogenic growth factor promoting tissue repair after myocardial infarction. *Circulation*. 2017;136(19):1809–1823.
47. Pleiner T, Tomaleri GP, Januszyk K, Inglis AJ, Hazu M, Voorhees RM. Structural basis for membrane insertion by the human ER membrane protein complex. *Science*. 2020;369(6502):433–436.
48. Bai L, You Q, Feng X, Kovach A, Li H. Structure of the ER membrane complex, a transmembrane-domain insertase. *Nature*. 2020;584(7821):475–478.
49. Shurtleff MJ, Itzhak DN, Hussmann JA, et al. The ER membrane protein complex interacts cotranslationally to enable biogenesis of multipass membrane proteins. *Elife*. 2018;7:e37018.
50. Miller-Vedam LE, Br auning B, Popova KD, et al. Structural and mechanistic basis of the EMC-dependent biogenesis of distinct transmembrane clients. *Elife*. 2020;9:e62611.

51. Li L, Jiao X, D'Atri I, et al. Mutation in the intracellular chloride channel CLCC1 associated with autosomal recessive retinitis pigmentosa. *PLoS Genet.* 2018;14(8):e1007504.
52. Dryja TP, Finn JT, Peng YW, McGee TL, Berson EL, Yau KW. Mutations in the gene encoding the alpha subunit of the rod cGMP-gated channel in autosomal recessive retinitis pigmentosa. *Proc Natl Acad Sci U S A.* 1995;92(22):10177–10181.
53. Kondo H, Qjin M, Mizota A, et al. A homozygosity-based search for mutations in patients with autosomal recessive retinitis pigmentosa, using microsatellite markers. *Invest Ophthalmol Vis Sci.* 2004;45(12):4433–4439.
54. Wycisk KA, Zeitz C, Feil S, et al. Mutation in the auxiliary calcium-channel subunit CACNA2D4 causes autosomal recessive cone dystrophy. *Am J Hum Genet.* 2006;79(5):973–977.
55. Hemara-Wahanui A, Berjukow S, Hope CI, et al. A CACNA1F mutation identified in an X-linked retinal disorder shifts the voltage dependence of Cav1.4 channel activation. *Proc Natl Acad Sci U S A.* 2005;102(21):7553–7558.
56. Besharse JC, Forestner DM, Defoe DM. Membrane assembly in retinal photoreceptors. III. Distinct membrane domains of the connecting cilium of developing rods. *J Neurosci.* 1985;5(4):1035–1048.
57. De RE. Electron microscope observations on the submicroscopic organization of the retinal rods. *J Biophys Biochem Cytol.* 1956;2(3):319–330.
58. Horst CJ, Johnson LV, Besharse JC. Transmembrane assemblage of the photoreceptor connecting cilium and motile cilium transition zone contain a common immunologic epitope. *Cell Motil Cytoskeleton.* 1990;17(4):329–344.
59. Lerea CL, Somers DE, Hurley JB, Klock IB, Bunt-Milam AH. Identification of specific transducin alpha subunits in retinal rod and cone photoreceptors. *Science.* 1986;234(4772):77–80.
60. Peng YW, Robishaw JD, Levine MA, Yau KW. Retinal rods and cones have distinct G protein beta and gamma subunits. *Proc Natl Acad Sci U S A.* 1992;89(22):10882–10886.
61. Baehr W, Devlin MJ, Applebury ML. Isolation and characterization of cGMP phosphodiesterase from bovine rod outer segments. *J Biol Chem.* 1979;254(22):11669–11677.
62. Hurley JB, Stryer L. Purification and characterization of the gamma regulatory subunit of the cyclic GMP phosphodiesterase from retinal rod outer segments. *J Biol Chem.* 1982;257(18):11094–11099.
63. Catty P, Pfister C, Bruckert F, Deterre P. The cGMP phosphodiesterase-transducin complex of retinal rods. Membrane binding and subunits interactions. *J Biol Chem.* 1992;267(27):19489–19493.
64. Li TS, Volpp K, Applebury ML. Bovine cone photoreceptor cGMP phosphodiesterase structure deduced from a cDNA clone. *Proc Natl Acad Sci U S A.* 1990;87(1):293–297.
65. Tsang SH, Burns ME, Calvert PD, et al. Role for the target enzyme in deactivation of photoreceptor G protein *in vivo*. *Science.* 1998;282(5386):117–121.
66. He W, Cowan CW, Wensel TG. RGS9, a GTPase accelerator for phototransduction. *Neuron.* 1998;20(1):95–102.